Research Square

Preprints are preliminary reports that have not undergone peer review.
They should not be considered conclusive, used to inform clinical practice,
or referenced by the media as validated information.

Preparation and Characterization of Hexagonal ZnO Nanoprisms Grown on the Surface of PAN Fiber Activated with Pd-Nanoparticles in a Wet Process

Jae-Young Lee

jjkle@naver.com

Hydrogen Fuel Cell Center, Woosuk University https://orcid.org/0000-0002-2430-6130

HONGKI LEE

Research Article

Keywords: ZnO nanoprism, ZnO plated PAN fiber, Palladium nanoparticle, H2S removal, Electroless plating, Tensile strength

Posted Date: November 9th, 2026

DOI: https://doi.org/10.21203/rs.3.rs-11456685/v1

License: This work is licensed under a Creative Commons Attribution 4.0 International License.
Read Full License

Preparation and Characterization of Hexagonal ZnO Nanoprisms Grown on the Surface of PAN Fiber Activated with Pd-Nanoparticles in a Wet Process

Jae-Young Lee[1] and Hong-Ki Lee[1,2]

[1]Hydrogen Fuel Cell Parts and Applied Technology Regional Innovation Center, Woosuk University, Jeollabuk-do, Korea
[2]Department of Hydrogen Energy Engineering, Woosuk University, Jeollabuk-do, Korea

Corresponding author: Jae-Young Lee
E-mail address: jjklee@naver.com
ORCID: 0000-0002-2430-6130

Abstract

Hexagonal zinc oxide (ZnO) nanoprisms grow on the surface of polyacrylonitrile (PAN) fiber in an electroless plating solution, where the surface of the PAN fiber was pre-activated with palladium (Pd) nanoparticles through a wet process. Pd-activation was performed by a spontaneous reduction of palladium(II) bis(acetylacetonate) on the surface of swollen PAN fiber in dimethylformamide/water solution at 90°C for various time, and it was found that ZnO nanoprisms grow site-selectively on the Pd nanoparticles through an energy filtering transmission electron microscopy. The morphology observation of hexagonal ZnO nanoprisms grown on PAN fiber surface was carried out by a field emission scanning electron microscopy (FE-SEM) and an X-ray photoelectron spectroscopy was used to evaluate their elemental composition. X-ray diffraction (XRD) patterns showed that the crystalline structure of ZnO nanoprisms was Wurtzite structure, and FE-SEM and XRD analyses showed that the length and covering of nanoprisms have become longer and wider as the electroless plating time increased. H_2S removal performance of the ZnO nanoprisms increased with increasing electroless reaction time and the saturated H2S uptake weight was 27.2 wt% of ZnO nanoprisms/PAN fiber prepared at 80°C for 120 min.

Keywords ZnO nanoprism · ZnO plated PAN fiber · Palladium nanoparticle · H_2S removal · Electroless plating · Tensile strength

Statements and Declarations

Competing interests

The authors declare that they have no competing interests.

Introduction

Polymer electrolyte membrane fuel cells (PEMFCs) are a preferred technology as a clean energy source that generates high power density at low operating temperature [1-3]. However, durability and reliability of the FEMFCs are being challenged by operating conditions such as fuel purity and oxidant concentration, and numerous reports have been published regarding the effect of contamination caused by these factors. Fuel contamination acts as a severe poisoning of platinum (Pt) nanocatalyst, critically affecting the proton conduction of the membrane, and the impurities in the oxidant affect the electrodes and membranes. Pt nanocatalysts dispersed on carbon supporter are ideal catalysts that act in both the hydrogen oxidation reaction (HOR) and the oxygen reduction reaction (ORR), however they are easily poisoned by contaminants in the reactants [4-7]. Contaminants include sulfur compounds (SO_2, carbonyl sulfide (COS), H_2S), carbon monoxide (CO), nitrogen compounds (NO_2, NO), ammonia, chlorides, and sulfates. These compounds must be removed using purification technologies prior to supply to PEMFCs, among which sulfur compounds have the most critical effect on fuel cell performance [8-10]. Therefore, it is necessary to maintain the sulfur concentration in the hydrogen fuel at 4 ppb [11,12].

In nature, hydrogen does not exist as a resource in a form usable as energy, instead, it mostly exists in the form of water (H_2O), ammonia (NH_3), and organic compounds (hydrocarbons such as methane (CH_4), ethane (C_2H_6), natural gas, etc., methanol (CH_3OH), ethanol (C_2H_5OH), biogas, etc.). Therefore, various studies are currently underway to separate and utilize hydrogen from these resources [13-15].

In order to produce hydrogen by splitting water molecules, 242 kJ/mol of energy is required theoretically, and this energy is supplied in the form of electricity, light or/and heat. Among these, water electrolysis method is most researched and is expected to have a bright future. This method is a very eco-friendly process because it produces only hydrogen and oxygen without pollutants. However, it has the disadvantage of requiring expensive electrochemical catalysts such as platinum (Pt), ruthenium (Ru) and iridium (Ir) [16-18].

The process of separating hydrogen from ammonia typically requires a cracking step involving heating at high temperature of 400-600℃ or higher, which consumes additional energy. Furthermore, ammonia itself is toxic and has a pungent odor, so a leak can have fatal effects on the environment and human health. Therefore, thorough safety management and equipment are essential. Additionally, to obtain high-purity hydrogen, a purification process is required to remove contaminants such as residual ammonia and nitrogen oxides (NOx) [19,20].

Representative methods for producing hydrogen from organic compounds include a reforming process and a

pyrolysis process [21-23]. In the reforming process, hydrogen is produced through the reaction of organic compounds with steam under catalytic condition at 700-1,000℃. Because this process is technically highly mature and has low production costs, most of hydrogen currently produced worldwide is manufactured using this method. However, this process inevitably generates large amounts of carbon dioxide (CO_2), a greenhouse gas, and also produces small amounts of carbon monoxide (CO), which acts as a catalyst poison. In the pyrolysis process, organic compounds are heated at high temperatures of 1,000℃ or higher to produce hydrogen along with solid carbon. Although this process does not produce CO_2, a phenomenon called coking occurs, where the generated solid carbon covers the catalyst surface, reducing its activity. Additionally, accumulated carbon can clog the reactor interior or piping, hindering the continuous process. In particular, the hydrogen produced by these two methods naturally contains sulfur compounds that act as catalyst poisons, and these compounds must be removed through a purification process to meet specification for sulfur content in hydrogen. This is because, in most countries, natural gas is managed to have a sulfur content of 30 ppm or less, gasoline and diesel are managed to have a sulfur content of 10 ppm. In addition, biogas contains sulfur ranging from 100 ppm to 10,000 ppm. These sulfur contents are still at a very high level for use as hydrogen (sulfur content of 4 ppb or less) in fuel cells [12,24-26].

Recently, SARS (selective adsorption for removing sulfur) technology is being used to remove trace amounts of sulfur compounds from reformed hydrogen [27-31]. Sulfur compounds contained in the reformed hydrogen is removed as it passes through an adsorbent layer composed of activated carbon, Fe-BEA zeolite or ZnO etc. In order to increase the sulfur removal performance, the contact area between solid adsorbents and sulfur compounds in gas state must be increased. To achieve this, (1) nickel (Ni), cobalt (Co), molybdenum (Mo), etc. are finely dispersed on a supporter (alumina, etc.) in sizes of 1-20 nm to maximize the surface area [27], (2) an adsorbent (such as zeolite, activated carbon, etc.) having a micropore structure with a size of 0.3-1 nm is used to selectively adsorb and remove gaseous sulfur compounds [28,29], or (3) a nano-sized ZnO is used as a chemical adsorbent at 200-400℃ [30,31].

It is well-known that nano-sized ZnO is used in a uniformly coated state on the surface of polymer textile fabrics for ease of handling. To coat a polymer surface with ZnO, the polymer surface should be pre-activated with palladium (Pd) seeds, and the best-known activation method consists of a combination of Sn and Pd chemical processes: $SnCl_2$ solution and $PdCl_2$ solution are mixed in HCl solution [32,33]. In our previous paper, we reported a Pd-activation method in a drying process in which sublimated palladium(II) bis(acetylacetonate), ($Pd(acac)_2$) was spontaneously reduced to Pd nanoparticles on the surface of a polyacrylonitrile (PAN) fiber at

180℃ in nitrogen atmosphere without using any reducing agent [34,35].

In this work, Pd-activation was performed by a spontaneous reduction of $Pd(acac)_2$ on the surface of swollen PAN fiber in wet process, and it was found that ZnO nanoprisms grow site-selectively on the Pd nanoparticles. Subsequently, the H_2S uptaking capacity of the self-manufactured ZnO was estimated.

Experimental part

Materials

$Pd(acac)_2$ was purchased from Johnson Matthey. It was recrystallized in acetone at 50℃ before use in order to remove impurities. N,N-dimethylformamide (DMF) and ethylene glycol (EG) were purchased from Duksan Pure Chemical Co., Ltd. (Korea). Zinc nitrate hexahydrate ($Zn(NO_3)_2 \cdot 6H_2O$) and dimethylamine borane (DMAB) were purchased from FUJIFILM Wako Pure Chemical Co. (Japan). PAN fiber was obtained from Tai'an Pole Geosynthetics Co., Ltd. (China). The diameter was 13±1 μm and it was chopped into a length of ca. 1 cm.

Pd-activation on the surface of PAN fiber in wet process

The surface of chopped PAN fiber was activated by Pd nanoparticles according to the following procedure in wet process: chopped PAN fiber (2g) was added and completely dispersed in DMF/distilled water (190g/10g) solution and then it became swollen by maintaining the mixture at 90℃ for 3 h. Subsequently, $Pd(acac)_2$ (0.03g) was dissolved and maintained at 90℃ for various time. During this process, $Pd(acac)_2$ molecules penetrated into the swollen surface of PAN fiber and was spontaneously reduced to Pd metallic nanoparticles, thereby activating the surface of the PAN fibers. The DMF and distilled water were removed using a vacuum filtration device, and the unreacted $Pd(acac)_2$ was removed by washing three times with acetone. The washed Pd-activated PAN fiber was then dried in a vacuum oven at 40℃ for 24 h. These were stored in a desiccator.

ZnO nanoprism growth on the Pd-activated PAN fiber

ZnO nanoprisms were grown on the Pd-activated surface of PAN fiber according to the following procedure: 0.05M-$Zn(NO_3)_2$ and 0.05M-DMAB were solved in EG/distilled water (20g/60g), and the Pd-activated PAN fiber (0.5g) was put into the solution. And then, ZnO nanoprisms grew on the Pd-activated PAN surface at 80℃ for various time (30-120 min). Finally, ZnO-grown PAN fiber was cleaned with distilled water and was dried in a 40℃ vacuum oven for 24 h. These were stored in a desiccator.

Instrumental analyses

To observe the Pd nanoparticles on the surface area of PAN fiber, energy-filtering transmission electron microscopy (EF-TEM, LEO922) was employed, and TEM image and elemental mapping data were observed. The morphology of ZnO nanoprisms were observed by field emission scanning electron microscopy (FE-SEM, JMS-6701F, JEOL) and the elemental analysis was carried out by energy-dispersive X-ray spectroscopy (EDS, JED-2300 Energy Dispersive X-ray Analyzer, JEOL). X-ray diffraction (XRD) analysis for ZnO nanoprisms was performed with a Bruker M18XCE diffractometer using a Cu-Kα source at 40 kV and 40 mA..

Measurement of H_2S uptake

The H_2S uptake performance of ZnO nanoprisms was measured by a thermogravimetric analyzer (TGA, Model: SDT Q600 (TA Instruments, Inc. USA)). 10 mg of ZnO nanoprisms grown on the PAN fiber was put into the electric furnace of TGA and dried at 250℃ for 12 h under nitrogen purging at 50 ml/min. Subsequently, the weight change due to H_2S uptake was measured while flowing a syngas composed of 69% nitrogen, 30% hydrogen and 1% H_2S at a flow rate of 20 ml/min.

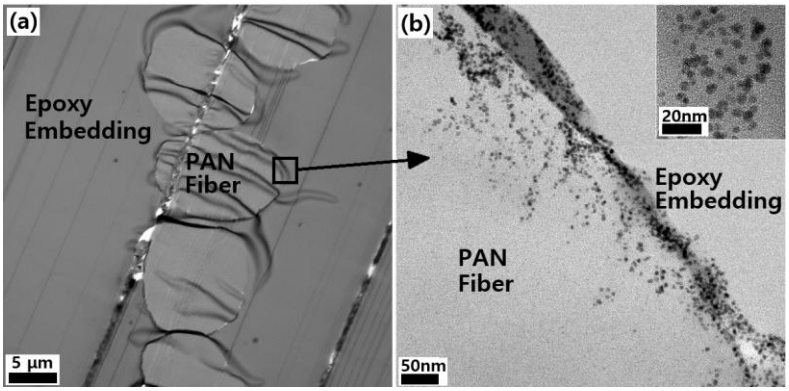


Fig. 1 (a) TEM cross-section image of Pd-activated PAN fiber and (b) TEM image of Pd nanoparticles formed near the surface of PAN fiber, which are prepared by spontaneous reduction of $Pd(acac)_2$ at 90℃ 120 min in wet process. The magnified TEM image inserted in (b) shows the morphology of Pd nanoparticles.

Results and discussion

Fig. 1(a) shows TEM cross-section image of Pd-activated PAN fiber embedded in epoxy resin and Fig. 1(b) shows TEM image of Pd nanoparticles formed near the surface of PAN fiber, which are prepared by the

reduction of $Pd(acac)_2$ at 90℃ 120 min in wet process. Almost all Pd nanoparticles are generated beneath the surface of the PAN fiber, and they are observed up to a depth of 292 μm from the surface. However, there is no Pd nanoparticle in deeper regions. The depth is approximately 8 times deeper than that of Pd nanoparticles prepared by our previous dry process [35], which is 37 μm. The synthetic mechanism of Pd nanoparticles beneath the surface of PAN fiber can be briefly explained as follows: $Pd(acac)_2$ molecules diffuse into the swollen PAN chains, adsorb to the nucleophilic -C≡N groups of the PAN fiber, and then spontaneously reduce to form Pd seeds, which grow to create Pd nanoparticles. Furthermore, in the dry process, it is difficult for $Pd(acac)_2$ molecules to penetrate into the high-density PAN fibers, whereas in the wet process, they diffuse relatively easily into the swollen PAN fibers, resulting in the formation of Pd nanoparticles in deeper regions. The inset of Fig. 1(b) shows the magnified morphology of Pd nanoparticles. The shape of Pd nanoparticles is spherical, and their size is 1.8-5.3 μm. Thus, the Pd nanoparticles can act as nuclei for the growth of ZnO nanoprisms.

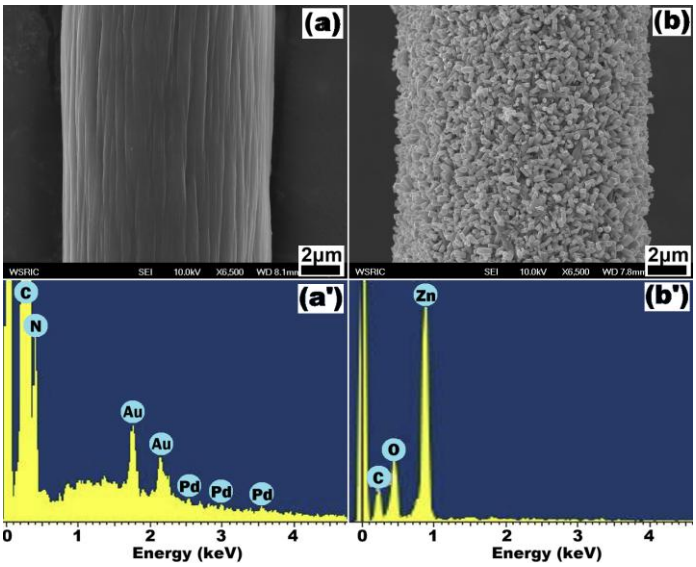


Fig. 2 SEM images with EDS spectra for (a, a') Pd-activated PAN fiber, which is prepared by spontaneous reduction of $Pd(acac)_2$ at 90℃ 60 min in wet process. and (b, b') ZnO nanoprisms grown on the Pd-activated PAN fiber, which are synthesized at 80℃ for 120 min in EG/distilled water solution of 0.05M-$Zn(NO_3)_2$ and 0.05M-DMAB.

SEM images and EDS spectra for (a, a') Pd-activated PAN fiber and (b, b') ZnO nanoprisms grown on the Pd-activated PAN fiber are shown in Fig. 2. Pd-activation is carried out by spontaneous reduction of $Pd(acac)_2$

at 90℃ 60 min in wet process, ZnO nanoprisms are synthesized at 80℃ for 120 min in EG/distilled water solution of 0.05M-$Zn(NO_3)_2$ and 0.05M-DMAB. These SEM images show that the surface of Pd-activated PAN fiber is covered by ZnO nanoprisms, and EDS spectrum of Fig. 2(a') show that the surface of PAN fiber is activated with Pd nanoseeds, where Au is attributed to the gold coating of the non-conductive PAN surface for TEM observation, and EDS spectrum of Fig. 2(b') shows that the elemental composition of Zn : O is 49.3 : 50.7 atomic % without Pd peaks, which means that the Pd-activated PAN fiber is fully covered by ZnO nanoprisms.

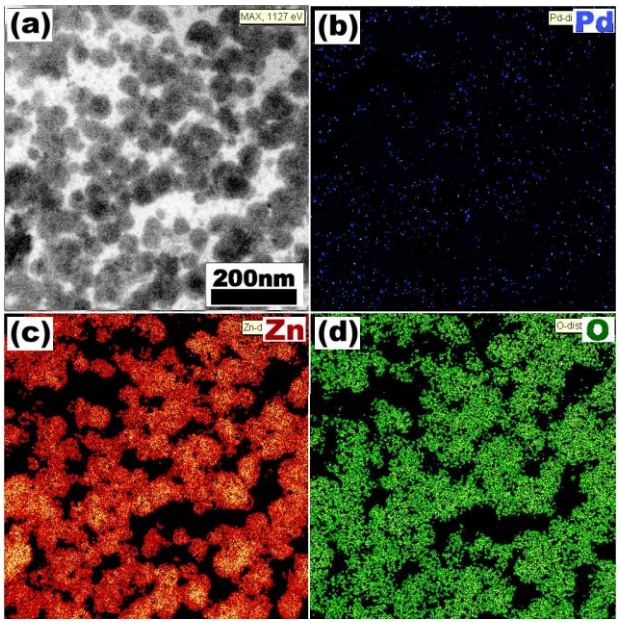


Fig. 3 (a) zero-loss image in EF-TEM and (b) Pd elemental map, (c) Zn elemental map and (d) O elemental map of ZnO nanoparticles grown on Pd nanoseeds. ZnO nanoparticles are synthesized at 80℃ for 30 min in EG/distilled water solution of 0.05M-$Zn(NO_3)_2$ and 0.05M-DMAB, where Pd-activation is prepared by spontaneous reduction of $Pd(acac)_2$ at 90℃ for 60 min in wet process.

To verify the selective growth of ZnO nanoparticles on Pd nuclei, EF-TEM and elemental mapping techniques are applied to the ZnO nanoparticles grown on the Pd-activated PAN surface. ZnO nanoparticles are synthesized at 80℃ for 30 min in EG/distilled water solution of 0.05M-$Zn(NO_3)_2$ and 0.05M-DMAB, where Pd-activation is preliminarily prepared by spontaneous reduction of $Pd(acac)_2$ at 90℃ for 60 min in wet process. In here, a thin PAN film with ZnO nanoparticles is prepared on the 600 mesh carbon-coated Cu grid, following the similar procedure explained in the experimental section: Chopped PAN fiber is completely dissolved in DMF solvent to be a concentration of 0.75 wt%. Then, ca. 20 nm thick PAN film is spin-coated on a cleaved NaCl

crystal and is dried in a 40℃ vacuum oven for 24 h. After drying, the PAN film is lifted off from the NaCl by dipping it into distilled water and is mounted on 600 mesh carbon-coated Cu grid. Pd-activation and ZnO deposition are carried out. An EF-TEM image is shown in Fig. 3(a) for the magnified ZnO nanoparticles and the corresponding elemental maps of Pd, Zn and O (Fig. 3(b), 3(c) and 3(d), respectively). These maps are precisely superimposed with the EF-TEM image, indicating that ZnO nanoparticles are site-selectively grown on Pd nanoseeds.

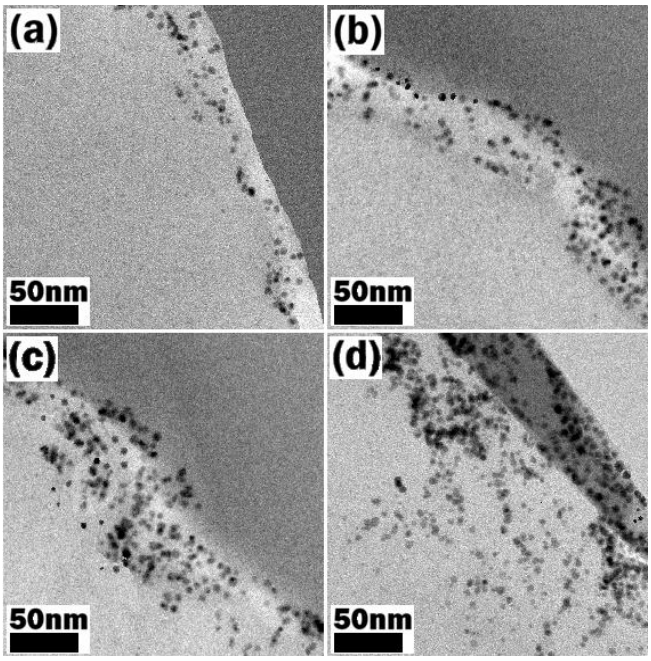


Fig. 4 TEM images of Pd nanoparticles formed near the surface of PAN fiber, which are prepared by spontaneous reduction of $Pd(acac)_2$ at 90℃ for various time in wet process. Pd-activation time: (a) 30 min, (b) 60 min, (c) 90 min and (d) 120 min.

Fig. 4 shows TEM images of Pd nanoparticles formed near the surface of PAN fiber, which are prepared by spontaneous reduction of $Pd(acac)_2$ at 90℃ for various time in wet process. Pd-activation time are (a) 30 min, (b) 60 min, (c) 90 min and (d) 120 min. If Pd-activation time increases, it can be seen that the distribution density of Pd nanoparticles increases and the penetration depth also increases. As confirmed in Fig. 3, since ZnO nanoparticles grow on Pd nanoseeds, it is necessary to focus on the dispersion state of the surface area. When the Pd-activation time is 30 min, it can be seen that there are many inactive regions on the surface of the PAN fiber, that is, regions where no nanoparticles are generated, and the dispersion density of the nanoparticles is low.

When the activation time is 60 min, almost all the entire surface is activated with Pd nanoparticles and its dispersion density increases slightly. If Pd-activation time is 120 min, all the surface of PAN fiber is activated and the dispersion density is very high.

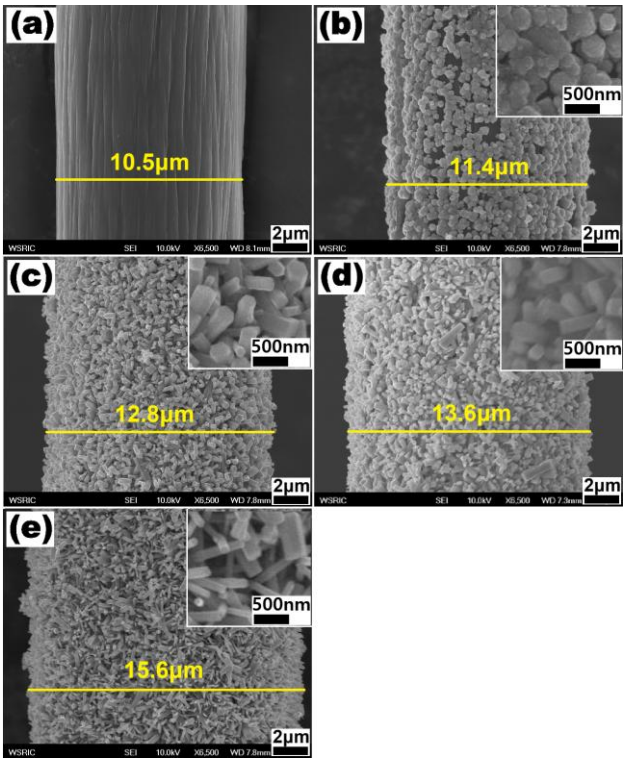


Fig. 5 SEM images of ZnO morphology grown on Pd-activated PAN fiber, which are prepared by spontaneous reduction of $Pd(acac)_2$ at 90℃ for various time in wet process. Pd-activation time is (a) 0 min, (b) 30 min, (c) 60 min, (d) 90 min and (e) 120 min. All ZnO nanoparticles are synthesized at 80℃ for 120 min in EG/distilled water solution of 0.05M-$Zn(NO_3)_2$ and 0.05M-DMAB. Each inset shows a high magnification image.

SEM images in Fig. 5 show the effect of Pd-activation time of PAN fibers on the morphology of ZnO nanoprisms. The Pd activation time is (a) 0 min, (b) 30 min, (c) 60 min, (d) 90 min and (e) 120 min. All ZnO nanoprisms are synthesized at 80℃ for 120 min in EG/distilled water solution of 0.05M-$Zn(NO_3)_2$ and 0.05M-DMAB. Each inset shows a high magnification image. As seen in Fig. 4, when the Pd activation time is 30 min, there is an inactivated region and the dispersion density of Pd nanoparticle is low, and therefore there is a region where ZnO nanoparticles are not grown (Fig. 5(b)), and the shape of the ZnO nanoparticles begins to appear as hexagonal nanoprisms. The diameter of the PAN fiber is 10.5 μm, and the diameter including the ZnO nanoparticles is 11.4 μm, so the length of the ZnO nanoprisms is 0.45 μm. When the Pd activation time is 60

min, almost all the surface is activated and the dispersion density of Pd nanoparticles increases, so all the surface is covered with hexagonal ZnO nanoprisms (Fig. 5(c)). The diameter of the PAN fiber including the ZnO nanoparticles is 12.8 μm, so the length of ZnO nanoprisms is 1.15 μm. If the Pd activation time is 120 min, all the surface is activated and the dispersion density of Pd nanoparticles is very high, so all the surface is covered with thinner hexagonal ZnO nanoprisms (Fig. 5(e)). The length of the ZnO nanoprisms is 2.55 μm, which is 5.7 times longer than that of 30 min-activation.

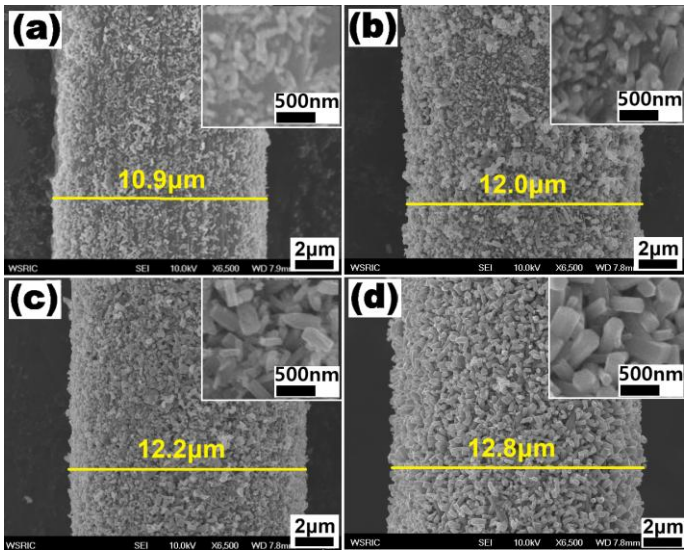


Fig. 6 SEM images of ZnO morphology synthesized at 80℃ for various time ((a) 30 min, (b) 60 min, (c) 90 min and (d) 120 min) in EG/distilled water solution of 0.05M-$Zn(NO_3)_2$ and 0.05M-DMAB. Pd-activation of PAN fiber is prepared by spontaneous reduction of $Pd(acac)_2$ at 90℃ for 60 min in wet process. Each inset shows a high magnification image.

Fig. 6 shows SEM images for ZnO nanoprisms grown on Pd-activated PAN fiber, where Pd-activation is prepared by spontaneous reduction of $Pd(acac)_2$ at 90℃ for 60 min in wet process. ZnO nanoprisms are synthesized at 80℃ in EG/distilled water solution of 0.05M-$Zn(NO_3)_2$ and 0.05M-DMAB for various time of (a) 30 min, (b) 60 min, (c) 90 min and (d) 120 min. As the synthetic time increases, the coverage of the PAN fiber surface by ZnO nanoprisms increases and the length the nanoprisms become longer. When the synthetic time is 30 min, the ZnO coverage is low and hexagonal ZnO nanoprisms is in the formation step, and when the synthetic time is 60 min, almost all the PAN fiber surface is covered with hexagonal ZnO nanoprisms, albeit small. As the electroless synthetic time increases, the coverage of ZnO nanoprisms increases, and their size

increases. When the reaction time is 120 min, the hexagonal ZnO nanoprisms are clearly shown in Fig. 6(d). The length of ZnO nanoprisms synthesized for 30 min, 60 min, 90 min, and 120 min is 0.2 μm, 0.75 μm, 0.85 μm, and 1.15 μm, respectively.

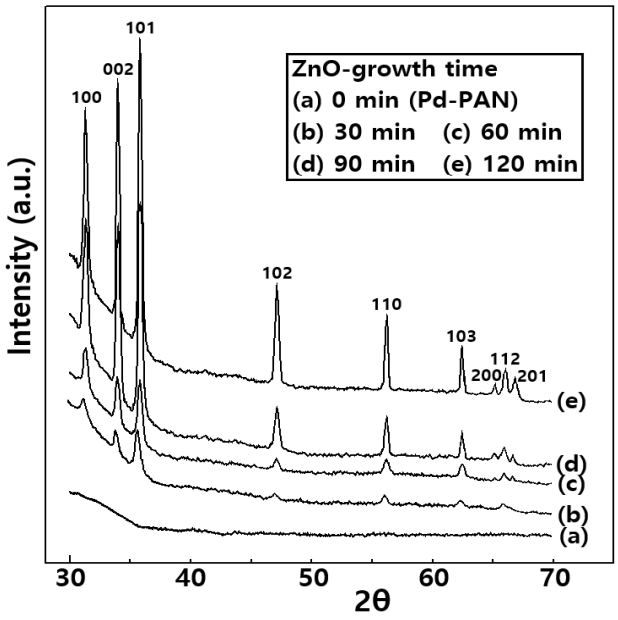


Fig. 7 XRD patterns for ZnO nanoprisms grown on Pd-activated PAN fiber prepared in an electroless solution at 80℃ for various times: (a) 0 min, (b) 30 min, (c) 60 min, (d) 90 min and (e) 120 min.

XRD analyses are carried out to study the crystalline structure of ZnO nanoprisms according to synthetic time and the patterns are shown in Fig. 7. ZnO nanoprisms grown on Pd-activated PAN fiber are synthesized in EG/distilled water solution of 0.05M-$Zn(NO_3)_2$ and 0.05M-DMAB at 80℃ for 0 min, 30 min, 60 min, 90 min and 120 min, respectively. Here, the Pd-activation of PAN fiber is prepared by spontaneous reduction of $Pd(acac)_2$ at 90℃ for 60 min in wet process. No peaks are observed in the XRD pattern of Pd-activated PAN fiber, that is, the PAN fiber with ZnO growth time of 0 min. The characteristic peaks of a neat PAN fiber show a main peak around 2θ = 17-18° and a weak auxiliary peak around 2θ = 29-30°, but since the XRD pattern in Fig. 7 is shown in the range of 2θ = 30-70°, only a portion of the broad peak is shown below 35°. As synthetic time increases, the characteristic peaks for the ZnO nanoprisms appear at 2θ = 31.6, 34.1, 36.1, 47.2, 56.4, 62.5 and 66.2°, and the intensity become strong. These peaks correspond to (100), (002), (101), (102), (110), (103) and (200) planes for ZnO nanoprisms, respectively. These peaks indicate that the crystalline structure is polycrystalline Wurtzite structure. In particular, when the synthetic time is short, the (200), (112), and (201)

peaks appear as a single broad band due to the overlap of incomplete phases (Fig. 7(b)), and when the synthetic time is sufficient, these three planes are clearly separated and distinctly displayed as sharp peaks. That is, at the beginning of the synthesis, growth occurs in the longitudinal direction, and when the synthetic time is sufficient, growth occurs in the thickening direction, forming a complete hexagonal crystalline structure [36].

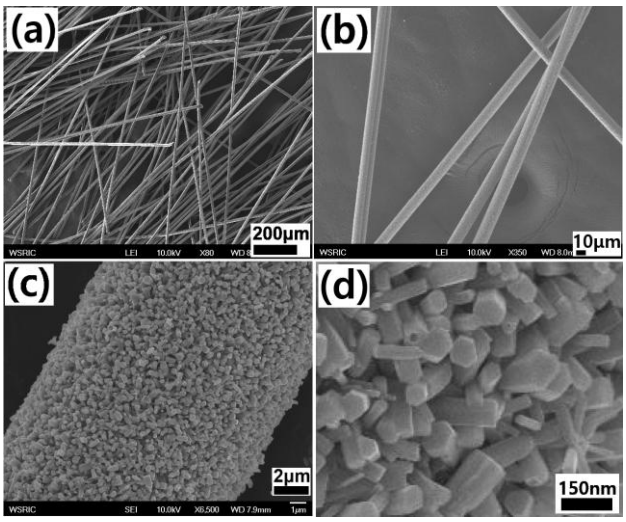


Fig. 8 SEM images for ZnO nanoprisms grown on Pd-activated PAN fiber prepared in an electroless solution at 80℃ for 120 min. The magnification is (a) ×80, (b) ×350, (c) ×6,500 and (d) ×200,000. Pd-activation of PAN fiber is prepared by spontaneous reduction of $Pd(acac)_2$ at 90℃ for 60 min in wet process.

To investigate the possibility of H2S removal of ZnO nanoprisms grown on the surface of PAN fabric, the fiber surface is preactivated with Pd nanoparticles through the spontaneous reduction of $Pd(acac)_2$ at 90℃ for 60 min in a wet process, and ZnO nanoprisms are synthesized in an electroless solution at 80℃ for 120 min. SEM images for the ZnO nanoprisms are shown in Fig. 8 and the magnification is (a) ×80, (b) ×350, (c) ×6,500 and (d) ×200,000. It is confirmed by SEM observation are uniformly covered on the surface of all PAN fibers, as shown in Fig. 8. As expected, the surface of all PAN fibers is evenly coated with ZnO (Fig. 8(a), 8(b) and 8(c)), and the ZnO morphology is hexagonal nanoprism-shape (Fig. 8(d)).

TGA analyses are carried out to study the H_2S uptake performance of the ZnO nanoprisms on the Pd-activated PAN fiber. The change in weight is measured while flowing synthesis gas containing 1% H_2S at a flow rate of 20 ml/min at an isothermal temperature of 250℃. The syngas contains N_2 69%, H_2 30% and 1% H_2S, and the weight change is shown in Fig. 9. As the ZnO-growth time increases, the H_2S uptake increases. When synthetic time is 120 min, in the initial state, H_2S uptake rate is very fast and the rate steeply decreases after 7 min. The

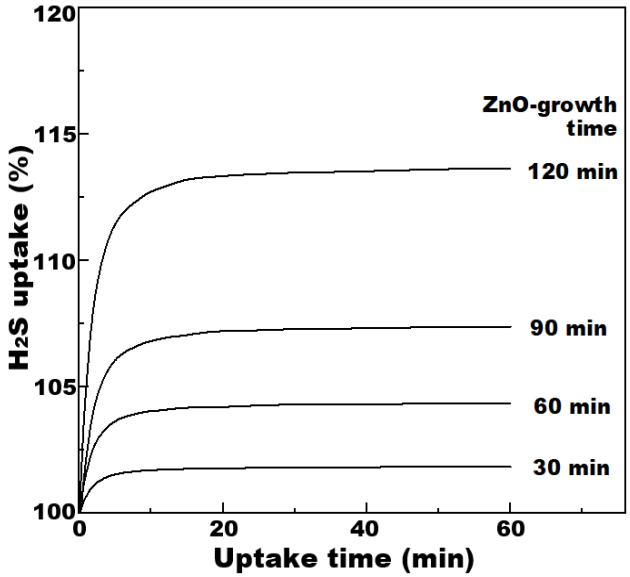


Fig. 9 TGA thermograms for H_2S uptake by ZnO nanoprisms grown on Pd-activated PAN fiber prepared in a reaction solution at 80℃ for various time.

saturated H_2S uptake weight is 13.6 wt% of ZnO/PAN fiber. The removal of H_2S using ZnO can be explained by the following mechanism: H_2S (gas) + ZnO (solid) → ZnS (solid) + H_2O (gas) [37]. Here, since S is substituted for O in a 1:1 ratio, and considering that the atomic weight of S is 32.06 g/mol and the atomic weight of O is 16.00/mol, the actual amount of sulfur removal must account for the weight loss due to oxygen and is 1.5 times the thermal weight loss. Therefore, the saturated H_2S uptake weight is 27.2 wt% of ZnO/PAN fiber, which is similar to the H2S uptake capacity of HiFUEL® A310 pellet (Johnson Matthey) [38]. Therefore, it is confirmed that the synthesized ZnO nanoprisms on PAN fiber can be used as adsorbent for the removal of sulfur compounds in hydrogen fuel cell applications.

Fig. 10 shows SEM images and EDS spectra of (a, a') ZnO nanoprisms and (b, b') ZnO-ZnS nanoparticles after H_2S uptake. ZnO nanoprisms are grown on Pd-activated PAN fiber prepared in an electroless solution at 80℃ for 120 min. Pd-activation of PAN fiber is prepared by spontaneous reduction of $Pd(acac)_2$ at 90℃ for 60 min in wet process. Comparing SEM images, it can be seen that ZnO nanoprisms are significantly collapsed and comparing EDS spectra, a new sulfur (S) peak appears in Figure 10(b'). The elemental composition of ZnO nanoprisms is Zn : O = 49.3 : 50.7 atomic %, and that of the nanoparticles after H_2S uptake is Zn : O : S = 49.5 : 21.6 : 28.9 atomic %. These results indicate the conversion of ZnO to ZnS and demonstrate that these ZnO nanoprisms can be used as a scavenger for sulfur compounds.

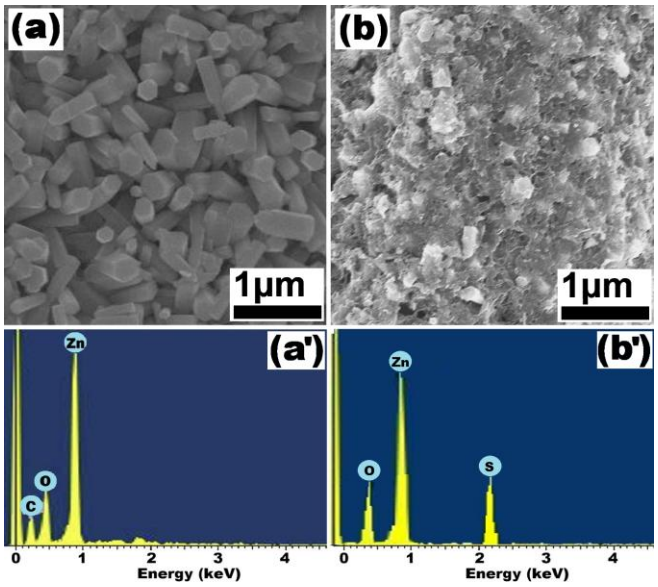


Fig. 10 SEM images with EDS spectra for (a, a') ZnO nanoprisms grown on the Pd-activated PAN fiber and (b, b') ZnO-ZnS nanoparticles after H_2S uptake.

Conclusion

Hexagonal ZnO nanoprisms grow on the surface of PAN fiber in an electroless plating solution, where the surface of the PAN fiber is pre-activated with Pd nanoparticles through a wet process. TEM observation shows that Pd nanoparticles with a size of 1.8-5.3 nm are generated beneath the surface of the PAN fiber, and the distribution density of the Pd nanoparticles increases, as Pd-activation time increases. EF-TEM and elemental map data show that ZnO nanoparticles are site-selectively grown on Pd nanoseeds. SEM observation shows that as the Pd-activation time increases, the coverage and length of ZnO nanoprisms on the PAN surface increase, while their thickness is found to be thinner. As the electroless reaction time increase, the coverage, length and thickness of ZnO nanoprisms on the PAN surface increase. When the reaction time is 120 min, all surface of the PAN fibers is covered with ZnO nanoprisms and the hexagonal ZnO nanoprisms are clearly shown. EDS spectrum shows that the elemental composition of Zn : O is 49.3 : 50.7 atomic % and XRD analysis shows the typical polycrystalline Wurtzite structure of ZnO nanoprisms and the intensity become strong, as the electroless reaction time increases. As the ZnO-growth time increases, the H_2S uptake increases. When synthetic time is 120 min, in the initial state, H_2S uptake rate is very fast and the rate steeply decreases after 7 min. The saturated H_2S uptake weight is 27.2 wt% of ZnO/PAN fiber. These results mean that the synthesized ZnO/PAN fiber can be used as an adsorbent for the removal of sulfur compounds for hydrogen fuel cell applications.

References

1. Alpaydin GU, Devrim Y, Colpan CO (2019) Performance of an HT-PEMFC having a catalyst with graphene and multiwalled carbon nanotube support. International Journal of Energy Research 43:3578-3589. https://doi.org/10.1002/er.4504
2. Zhou YD, Guo WJ, Xing LX et al (2025) Stability/durability challenges of cathode catalysts for PEM fuel cells: experiments, mechanisms, and perspectives beyond three-electrode systems. Energy and Environmental Science 18:9054-9092. https://doi.org/10.1039/d5ee03461b
3. Laghryb I, Malki M, Steiner NY et al (2025) Catalyst degradation in proton exchange membrane fuel cells: Mechanisms, investigation techniques, and predictive modelling. International Journal of Hydrogen Energy 145:496-507. https://doi.org/10.1016/j.ijhydene.2025.06.052
4. Gremminger A, Lott P, Merts M et al (2017) Sulfur poisoning and regeneration of bimetallic Pd-Pt methane oxidation catalysts. Applied Catalysis B: Environmental 218:833-843. https://doi.org/10.1016/j.apcatb.2017.06.048
5. Rohde S, Cowley A, Hasso R et al (2026) Influence of the electrode fabrication method on the resistance of PEM fuel cells to H_2S contamination. Journal of Power Sources 662:238698. https://doi.org/10.1016/j.jpowsour.2025.238698
6. Liu Y, Du L, Kong F et al (2020) Sulfur dioxide-tolerant bimetallic PtRu catalyst toward oxygen electroreduction. ACS Sustainable Chemistry & Engineering 8:1295-1301. https://doi.org/10.1021/acssuschemeng.9b06785
7. Morooka T, Shishido T, Nakanishi T et al (2025) Modification of platinum surfaces with cerium species for promoting oxidative desorption of adsorbed sulfur. Electrochemistry Communications 180:108050. https://doi.org/10.1016/j.elecom.2025.108050
8. Ali FSM, Daniel L, Heikkinen N et al (2025) Influence of contaminants on PEMFC performance – a multisinglecell approach. Next Research 2:100209. https://doi.org/10.1016/j.nexres.2025.100209
9. Chen HB, Zhang JS, Zhang HW et al (2025) Effect of Cation Contamination of Gas Diffusion Layer on Water Management and Performance of PEMFCs. Carbon Energy 7:e70038. https://doi.org/10.1002/cey2.70038

10. Li S, Zhu JK, Yang G et al (2025) A Review on Impact of the Marine Salt Spray Environment on the Performance of Proton Exchange Membrane Fuel Cells. Journal of Marine Science and Engineering 13:179. https://doi.org/10.3390/jmse13010172

11. Yang Y, Wang YH, Gao FY et al (2025) An Efficient H_2S-Tolerant Hydrogen Oxidation Electrocatalyst Enabled by a Lewis Acid Modifier for Fuel Cells. Nano Letters 25:3620–3629. https://doi.org/10.1021/acs.nanolett.4c06621

12. International Organization for Standardization. (2025). Hydrogen fuel quality — Product specification (ISO Standard No. 14687.

13. Dash SK, Chakraborty S, Elangovan D (2023) A Brief Review of Hydrogen Production Methods and Their Challenges. Energies 16:1141. https://doi.org/10.3390/en16031141

14. Li R, Kawanami H (2023) A Recent Review of Primary Hydrogen Carriers, Hydrogen Production Methods, and Applications. Catalysts 13:562. https://doi.org/10.3390/catal13030562

15. Kadam RS, Yadav GD (2024) Life cycle analysis of ammonia and methane production using green hydrogen and carbon dioxide. Journal of Cleaner Production 449:141620. https://doi.org/10.1016/j.jclepro.2024.141620

16. Bonanno M, Müller K, Bensmann B et al (2024) Review and Prospects of PEM Water Electrolysis at Elevated Temperature Operation. Advanced Materials Technologies 9:2300281. https://doi.org/10.1002/admt.202300281

17. Wang TZ, Cao XJ, Jiao LF (2022) PEM water electrolysis for hydrogen production: fundamentals, advances, and prospects. Carbon Neutrality 1:21. https://doi.org/10.1007/s43979-022-00022-8

18. Groenemans H, Saur G, Mittelsteadt C et al (2022) Techno-economic analysis of offshore wind PEM water electrolysis for H_2 production. Current Opinion in Chemical Engineering 37:100828. https://doi.org/10.1016/j.coche.2022.100828

19. Rizi HAY, Shin DH (2022) Green Hydrogen Production Technologies from Ammonia Cracking. Energies 15:8246. https://doi.org/10.3390/en15218246

20. Devkota S, Cha JY, Shin BJ et al (2024) Techno-economic and environmental assessment of hydrogen

production through ammonia decomposition. Applied Energy 358:122605. https://doi.org/10.1016/j.apenergy.2023.122605

21. Noh WJ, Lee IK (2024) Synergizing autothermal reforming hydrogen production and carbon dioxide electrolysis: Enhancing the competitiveness of blue hydrogen in sustainable energy systems. Chemical Engineering Journal 499:156688. https://doi.org/10.1016/j.cej.2024.156688
22. Hong SY, Lee JW, Cho HT et al (2022) Multi-objective optimization of CO_2 emission and thermal efficiency for on-site steam methane reforming hydrogen production process using machine learning. Journal of Cleaner Production 359:132133. https://doi.org/10.1016/j.jclepro.2022.132133
23. Liu S, Du PZ, Jia HK et al (2024) Study on the impact of methanol steam reforming reactor channel structure on hydrogen production performance. Renewable Energy 228:120612. https://doi.org/10.1016/j.renene.2024.120612
24. Cha YH, Mun SY, Lee KB (2023) Development of modified zeolite for adsorption of mixed sulfur compounds in natural gas by combination of ion exchange and impregnation. Applied Surface Science 619:156634. https://doi.org/10.1016/j.apsusc.2023.156634
25. Qiao Z, Chen Z, Gong H et al (2025) Enhancement of anaerobic digestion by adding elemental sulfur. Bioresource Technology 416:131820. https://doi.org/10.1016/j.biortech.2024.131820
26. Ma X, Sun L, Song C (2002) A new approach to deep desulfurization of gasoline, diesel fuel and jet fuel by selective adsorption for ultra-clean fuels and for fuel cell applications. Catalysis Today 77:107-116. https://doi.org/10.1016/S0920-5861(02)00237-7
27. Knudsen KG, Cooper BH, Topsøe H (1999) Catalyst and process technologies for ultra low sulfur diesel. Applied Catalysis A: General 189:205-215. https://doi.org/10.1016/S0926-860X(99)00277-X
28. Zhou N, Huang X, Zhang Y et al (2018) High performances of mesoporous g-C_3N_4 for adsorptive desulfurization in model gasoline (iso-octane) solutions. Applied Surface Science 448:636-641. https://doi.org/10.1016/j.apsusc.2018.04.084
29. Jafarabadi H, Mansouri M, Shayanmehr M et al (2025) Mechanisms, challenges, and future perspectives of

adsorptive desulfurization using zeolite-based adsorbents: a review. Environmental Science and Pollution Research 32:11350-11402.
https://doi.org/10.1007/s11356-025-36333-3

30. Ullah R, Tuzen M (2023) Facile hydrothermal synthesis of ZnO nanoparticles on silicalite-1: Effect of ultra ZnO Nano size on desulfurization activities. Surfaces and Interfaces 39:102918.
https://doi.org/10.1016/j.surfin.2023.102918

31. Sun H, Chen C, Zhang R et al (2025) Advances in Gasoline Hydrodesulfurization Catalysts: The Role of Structure-Activity Relationships and Machine Learning Approaches. ACS Omega 10:31262-31273.
https://doi.org/10.1021/acsomega.5c02980

32. Vijay S, Rao Ch.S (2019) Optimization of nickel deposition on boron carbide particles using design of experiments. Materials Today: Proceedings 18:4421-4430.
https://doi.org/10.1016/j.matpr.2019.07.411

33. Sun Z, Huang J (2019) Fabrication of nickel coating on polyethylene terephthalate substrate modified with primer: effect of surface roughness on structural properties of plated coating. Journal of Electronic Materials 48:6298-6305.
https://doi.org/10.1007/s11664-019-07291-7

34. Lee JY, Lee HK (2018) Electroless Ni-P metallization on palladium activated polyacrylonitrile (PAN) fiber by using a drying process. Materials Chemistry and Physics 204:257-261.
https://doi.org/10.1016/j.matchemphys.2017.10.048

35. Lee JY, Lee HK (2021) Preparation and characterization of ZnO nanorods grown on Pd-activated polyacrylonitrile (PAN) fiber. Materials Science and Engineering B 263:114821.
https://doi.org/10.1016/j.mseb.2020.114821

36. González-Fernández JV, Pinzón-Moreno DD, Neciosup-Puican AA et al (2022) Green Method, Optical and Structural Characterization of ZnO Nanoparticles Synthesized Using Leaves Extract of *M. oleifera*. Journal of Renewable Materials 10:833-847.
https://doi.org/10.32604/jrm.2021.017377

37. Ding P, Xu D, Huang H et al (2018) ZnS modified ZnO nano-heterojunction for efficient trace H_2S gas detection. IOP Conf. Series: Materials Science and Engineering 452:022031.
https://doi.org/10.1088/1757-899X/452/2/022031

38. Lorreyte C, Malinowska B, Butin V et al (2024) New Approach for Sulfidation Process in Packed Bed with

Hi-Fuel A310 Sorbent - Thermodynamical Studies. ChemEngineering 8:38.

https://doi.org/10.3390/chemengineering8020038

Acknowledgement

This work was financially supported by Institute for Korea Planning & Evaluation Institute of Industrial Technology Promotion (KEIT) grant funded by the Korea government (MOTIR) (No.2001249, Development of muticoating electrodes and MEA componentization technology for fuel cells that can be reduced by 40% for platinum use).

Funding

No funding was received for conducting this study.

Author contributions

Jae-Young Lee contributed to conceptualization, methodology, investigation, and manuscript drafting. Hong-Ki Lee contributed to conceptualization, investigation and data curation. All authors read and approved the final manuscript.

Ethics declarations

Ethics approval

Not applicable

Consent to participate

Not applicable

Consent for publication

Not applicable

Clinical trial number

Not applicable.

Competing interests

The authors declare that they have no competing interests.

Data availability

The data related to the current study is presented in the paper.